JOURNAL OF QUATERNARY SCIENCE (2026) 1–13 ISSN 0267-8179. DOI: 10.1002/jqs.70057

JQS Journal of Quaternary Science QRA Quaternary Research Association

From Ice to Isolation: A geochemical reconstruction of the palaeoenvironmental evolution of Gairloch, NW Scotland (UK), since the Last Glacial Maximum

JENNIFER TAYLOR,[1]* DAVID SELBY,[1] JEREMY M. LLOYD,[2] LOUISE BEST,[3] LUCA PODRECCA,[4] BRADLEY B. SAGEMAN[4] and ALEXANDER R. SIMMS[5]

[1]Department of Earth Sciences, Durham University, Durham, UK
[2]Department of Geography, Durham University, Durham, UK
[3]School of Education and Science, University of Gloucestershire, Cheltenham, UK
[4]Department of Earth and Planetary Sciences, Northwestern University, Evanston, IL, USA
[5]Department of Earth Science, University of California, Santa Barbara, CA, USA

Received 20 March 2025; Revised 4 February 2026; Accepted 9 February 2026

ABSTRACT: Complex relative sea-level (RSL) changes are associated with the deglaciation of the British and Irish Ice Sheet (BIIS). Sediment archives from Loch Bad na h-Achlaise, an isolation basin in NW Scotland, UK, span Late Glacial to Holocene time and record sea-level change and ice proximity via a geochemical and biostratigraphic multiproxy approach. Osmium and carbon isotope, carbon and nitrogen content, and X-ray fluorescence (XRF) data suggest that the basal sedimentary unit reflects a glaciomarine depositional setting, a finding previously unresolved due to an inadequate biostratigraphic framework. The $^{187}Os/^{188}Os$ record from the basin captures the RSL history of this site and illustrates the interplay between the local signal of glacial isostatic adjustment and the non-local signal of glacio-eustatic sea-level rise. By coupling the $^{187}Os/^{188}Os$ data with a detailed age–depth model, our study demonstrates a period of RSL fall between 16.2 and 15.9 cal ka BP, which culminates in basin isolation. The close agreement between the biostratigraphy, where available, and the $^{187}Os/^{188}Os$ record confirms the viability of this isotope system as an RSL proxy not reliant on microfossil preservation and thus a potentially effective approach when poor microfossil preservation hampers palaeoenvironmental reconstruction.

KEYWORDS: Gairloch; Holocene; Late Glacial; Loch Bad na h-Achlaise; Older Dryas; osmium-isotopes ($^{187}Os/^{188}Os$); palaeoenvironment

Introduction

The complex deglacial history of the British and Irish Ice Sheet (BIIS), which was present over much of the British Isles during the Last Glacial Maximum (LGM), provides insight into the relative contributions of glacial isostatic adjustment (GIA) and glacio-eustatic sea-level change on local relative sea-level (RSL) records (Flemming, 1982; Shennan et al., 2006a, 2006b; Smith et al., 2019). Recent studies have focused on defining the history of the BIIS and have documented the rapid retreat of several of the former ice streams draining its margins (Bradwell et al., 2019, 2021; Scourse et al., 2019; Clark et al., 2022). The study of the BIIS is of particular importance, as it may be useful as an analogue for the deglaciation of marine-influenced ice sheets (Clark et al., 2012). Northwest Scotland is well suited to RSL reconstructions due to the abundance of sedimentary archives, some of which are from isolation basins, which provide detailed palaeoenvironmental records and RSL index points (Shennan et al., 2000, 2006b; Bradley et al., 2011; Kuchar et al., 2012; Hamilton et al., 2015; Long et al., 2016; Best et al., 2022; Huffman et al., 2025). The longest and most complete RSL record for the British Isles is from Arisaig, NW Scotland (Shennan et al., 2005; Best and Shennan, 2024); RSL histories in this region reflect varied patterns of GIA, and data can be used to test GIA models. By refining models of land uplift and sea-level trends, such studies can improve global sea-level models and therefore projections of future sea-level rise.

Reconstruction of the palaeoenvironmental histories of such sites has traditionally relied on microfossil archives such as diatom and foraminiferal assemblages (e.g., Lloyd, 2000; Lloyd and Evans, 2002; Shennan et al., 2005; Hamilton et al., 2015). However, poor preservation can hamper such reconstructions, highlighting the need for palaeoenvironmental reconstructive methods not reliant on microfossil preservation. Together with traditional geochemical proxies ($\delta^{13}C$, C, N, and XRF data), this study uses the Os isotope system as a proxy to reconstruct the palaeoenvironmental history of an isolation basin, Loch Bad na h-Achlaise. The Os isotope system is attractive when studying palaeoceanographic changes, as its short residence time in seawater (10^3–10^4 years: Peucker-Ehrenbrink and Ravizza, 2000) allows temporally short fluctuations to be identified. The osmium isotope signature of the water column is captured in organic carbon-bearing sediments at the time of deposition (e.g., Ravizza and Turekian, 1989; Cohen et al., 1999; Kuroda et al., 2016; Peucker-Ehrenbrink and Ravizza, 2000; Paquay and Ravizza, 2012; Rooney et al., 2016). The ratio of $^{187}Os/^{188}Os$ in modern oceans is ~1.04–1.06, reflecting the balance of two sources (e.g., Sharma et al., 1997; Levasseur et al., 1998; Peucker-Ehrenbrink and Ravizza, 2000; Gannoun and Burton, 2014;

*Correspondence: J. Taylor, as above.
Email: jtaylor98@hotmail.co.uk

Rooney et al., 2016). The first source includes submarine volcanism, hydrothermal vents and cosmic dust, which yield unradiogenic sources of Os with $^{187}Os/^{188}Os$ ratios of 0.12 (Peucker-Ehrenbrink and Ravizza, 2000). The second source is riverine input, with the weathering of the upper continental crust yielding radiogenic sources of Os with $^{187}Os/^{188}Os$ values averaging ~1.4 and old crystalline rocks recording ratios of >2 (Peucker-Ehrenbrink and Ravizza, 2000; Peucker-Ehrenbrink and Jahn, 2001). As a result of these two distinct sources, the signature of marine water is distinct from that of freshwater. While the bedrock composition of the catchment of rivers strongly influences riverine compositions of Os, estimates of modern rivers suggest average $^{187}Os/^{188}Os$ values of ~1.2–1.5, more radiogenic than the modern ocean (Levasseur et al., 1999; Peucker-Ehrenbrink and Ravizza, 2000; Peucker-Ehrenbrink, 2002; Lu et al., 2017). Therefore, this isotope system is potentially useful in understanding the palaeoenvironmental history of isolation basins and has been successfully applied to Loch Duart, an isolation basin in NW Scotland (Taylor et al., 2024).

This multiproxy investigation from Loch Bad na h-Achlaise, Scotland, integrating C/N, $\delta^{13}C_{org}$, $^{187}Os/^{188}Os$ and X-ray fluorescence (XRF), adds significant detail to the palaeoenvironmental reconstruction, and the relative sea-level history of the region based on the microfossil framework of Simms et al. (2022). We demonstrate that the $^{187}Os/^{188}Os$ record aligns closely with biostratigraphic reconstructions and provides a refined understanding of the glaciological setting that captures the interplay between glacial isostatic adjustment and glacioeustatic sea-level change. This multiproxy geochemical approach enhances our capacity to resolve past environmental and RSL variability and represents a powerful strategy for application at other sites lacking robust biostratigraphic constraints.

Geographical and geological setting

Loch Bad na h-Achlaise is an isolation basin located in the Gairloch region of NW Scotland, UK (Fig. 1). The Applecross Formation of the Torridon Group comprises much of the bedrock of this locale, with the northeastern edge of the region dominated by Late Archean Lewisian Gneiss (Jonk et al., 2004). Glacial cycles have reworked the coastal regions of NW Scotland into characteristic 'knock- and lochan' topography, producing a setting ideal for isolation basin/lake development (Krabbendam and Bradwell, 2014). Such isolation basins preserve changes in RSL by recording periods of connection to and isolation from the open sea; basins located above the highest astronomical tide (HAT) accumulate freshwater sediments, while lower lying basins periodically inundated during the tidal cycle preserve brackish to marine sediments (Lloyd, 2000; Lloyd and

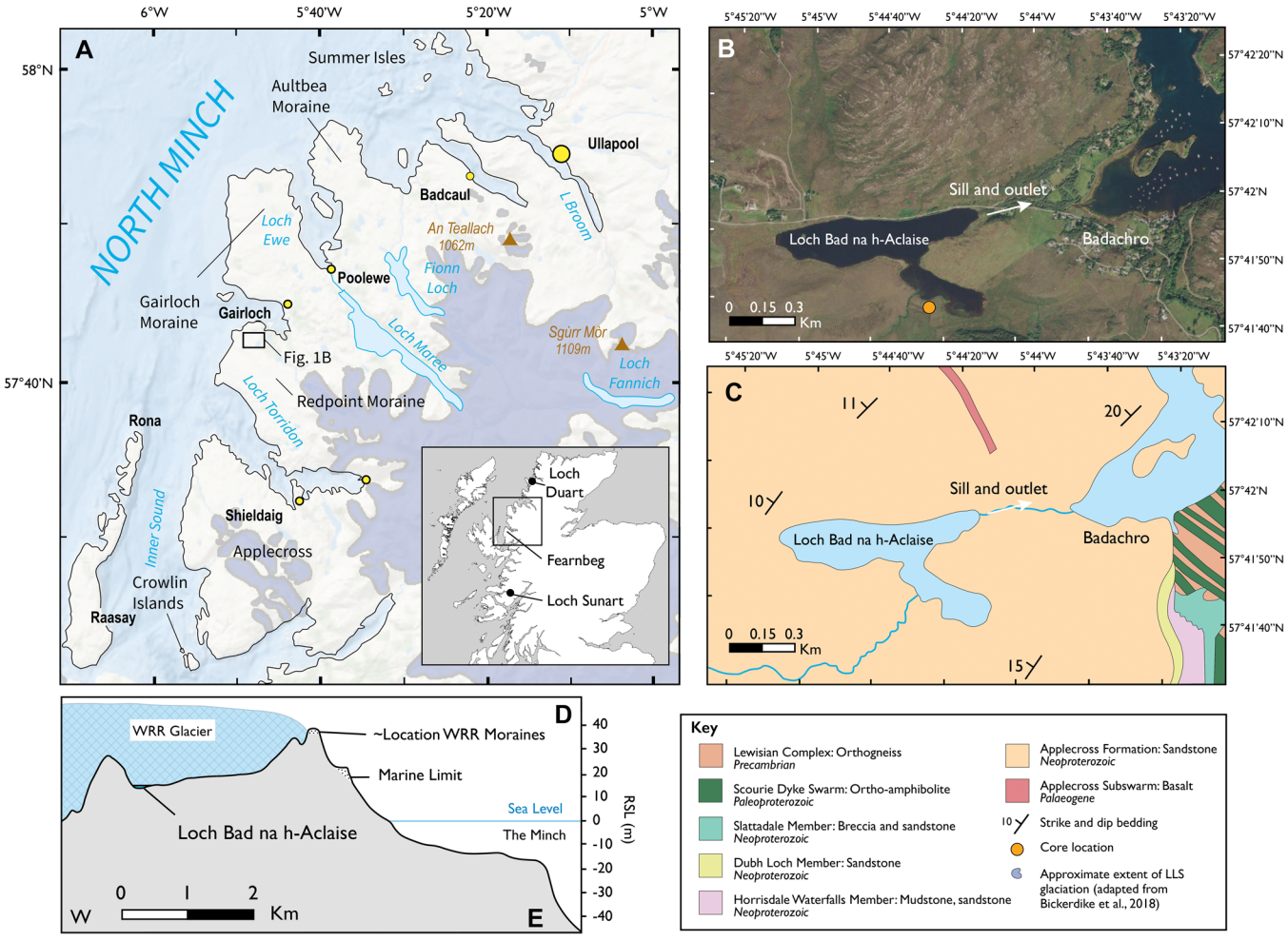

Figure 1. (A) Regional map of the area surrounding the study site, with key locations marked. The approximate extent of the Loch Lomond Stadial (LLS) glaciation (Younger Dryas) is marked in blue from Bickerdike et al. (2018). (B) Aerial image of the Loch Bad na h-Achlaise study site. The orange circle encompasses the sites of both cores: LBA18-11R and LBA23-11Q. (C) Geological map showing Loch Bad na h-Achlaise and its surrounding geology created using BGS Scotland map sheet 91. (D) Topographic profile through the study area showing the position of Loch Bad na h-Achlaise, the Wester Ross Readvance moraines and shorelines marking the marine limit (adapted from Simms et al., 2022). [Color figure can be viewed at wileyonlinelibrary.com]

Evans, 2002). At the present day, Loch Bad na h-Achlaise is an ~0.2 km^2 lochan (small lake) situated ~13.5 m above sea level. The lochan is connected to the ocean through a 500-m-long east-flowing outlet stream that runs into a small cove within Loch Gairloch (Fig. 1).

Materials and methods

This study utilises core LBA18-11R, which was obtained along the southwestern shore of Loch Bad na h-Achlaise (Simms et al., 2022; Fig. 1). An additional nearby core (<20 m), LBA23-11Q, was utilised for XRF scanning of selected sections (Section 3.3). Both cores were collected using a Russian corer. The elevation of the sill separating Loch Bad na h-Achlaise from the ocean is 12.65 ± 0.05 m ordnance datum (Simms et al., 2022). The altitude and elevation of the basin's sill were surveyed with a Leica 1200 differential GPS and Leica Automatic Optical Level in reference to Ordnance Survey benchmarks, giving elevations to Ordnance Datum Newlyn (m OD) (Simms et al., 2022). The sedimentary succession at Loch Bad na h-Achlaise spans from the Late Glacial through the Holocene and records glacial, marine and lacustrine deposition associated with a dynamic glacial and RSL history (Simms et al., 2022).

Sampling

Core LBA18-11R, spanning from subsurface depths of 225 to 630 cm, comprises 11 overlapping Russian core sections collected from the southern shore of Loch Bad na h-Achlaise (Simms et al., 2022; Fig. 1; Table S1). An additional 13 gouge cores were taken near the outlet stream of Loch Bad na h-Achlaise to survey the elevation of the sill separating it from the sea (Simms et al., 2022).

Age–depth model

An age–depth model for the LBA18-11R core was created using the BACON age–depth modelling software package (version 3.3.0) in R (version 4.4.1) (Blaauw and Christen 2011) from seven AMS ^{14}C ages obtained by Simms et al. (2022) using the IntCal20 calibration curve (Fig. 2; Table S2).

X-ray fluorescence (XRF)

XRF core scanning requires a flat, undisturbed surface for accurate analysis. Therefore, as core LBA18-11R had been previously sampled (Simms et al., 2022), the four core sections that comprise the nearby core (<20 m) LBA23-11Q were utilised for XRF scanning. The two cores were stratigraphically correlated using the key lithological contacts and units of each core (Fig. 3). Core sections from subsurface depths of 250–300, 350–400, 500–550 and 550–600 cm were scanned using the Geotek X-ray fluorescence (MSCL-XRF) spectrometer in the Department of Geography at Durham University. The 500–550 and 550–600 cm core sections were chosen, as they contain the previously identified isolation contact based on diatoms and the variations in clastic material towards the base of the core. The 250–300 and 350–400 cm core sections were utilised to investigate the variability between organic and clastic units identified from the stratigraphy within the freshwater section of the core.

The instrument provided high-resolution elemental abundance data from sediment core surfaces, achieving down- and across-core resolutions of 1 and 5 mm, respectively. The XRF spectrometer operates by bombarding the samples with high-energy X-rays generated in the rhodium X-ray tube. Elements ranging from Mg to U were detectable at ppm levels, with most achieving detection limits better than 20 ppm. To improve the sensitivity of light element measurements such as magnesium, aluminium and silicon, a silicon drift detector combined with a helium-flushed measurement cell was used. Data processing was carried out using the MSCLXYZ Core Workstation.

Carbon and nitrogen analyses

Regularly spaced core sediment samples ($n = 21$) were analysed for the stable isotope ratio of organic carbon ($\delta^{13}C_{org}$) alongside the overall carbon and nitrogen content (wt% C and N; see Table 1 for data synopsis). An aliquot of sample powder was acidified with 10% HCl to remove any carbonate. All samples were analysed using a Costech 4010 Elemental Analyser coupled to a Thermo Delta V+ mass spectrometer via a Conflo IV interface at the Northwestern Stable Isotope Biogeochemistry Laboratory (NUSIBL) at Northwestern University, USA. Samples were combusted over a column of Cr2O3 held at 980°C and a Cu reduction column held at 705°C. Elemental information was estimated via cross-calibration with acetanilide organic standards, and isotopic data $\delta^{13}C_{org}$ was determined via repeated analyses of Indiana University acetanilide ($\delta^{13}C = -29.52‰$) and urea standards ($\delta^{13}C = -8.01‰$) (Schimmelmann et al., 2009). Carbon isotopes are reported with respect to Vienna Pee Dee Belemnite (VPDB), with an overall uncertainty of 0.12‰.

Re and Os analysis

The Re–Os analysis was conducted at the Durham University (UK) Geochemistry Centre (Laboratory for Sulphide and Source Rock Geochronology and Geochemistry and Arthur Holmes Laboratory) on core LBA18-11R ($n = 31$). Agate powdered samples (1 g) were placed in Carius tubes and spiked with a known quantity of mixed ^{190}Os and ^{185}Re tracer solution along with 8 mL of Cr^{VI}–H_2SO_4 solution and heated at 220°C for 48 h (Selby and Creaser 2003). The Os was purified using solvent extraction ($CHCl_3$) with back extraction into HBr, and CrO_3–H_2SO_4–HBr micro-distillation. The Re fraction was purified using NaOH–C_3H_6O solvent extraction and anion chromatography. The Re and Os fractions were loaded onto Ni and Pt filaments, respectively. Isotopic measurements were performed using a ThermoScientific TRITON mass spectrometer via static Faraday collection for Re, and ion counting was conducted using a secondary electron multiplier in peak-hopping mode for Os. The total analytical protocol blanks are 12.73 ± 2 ppt for Re and 0.1 ± 0.02 ppt for Os, with a $^{187}Os/^{188}Os$ ratio of 0.24 ± 0.03; 1 SD ($n = 7$). A synopsis of the Re–Os data is presented in Table 1. To monitor the long-term reproducibility of the Re–Os isotope composition determinations, Re and Os solution standards are routinely analysed. At the time of analysis completion (June 2024), the Durham Romil Osmium Standard (DROsS: 50 pg solution) yielded a running average of 0.16084 ± 0.00059 (1 SD, $N = 1043$) for $^{187}Os/^{188}Os$ values and the rhenium standard solution (Restd: 125 pg solution) yielded a running average of 0.59861 ± 0.0015 (1 SD, $N = 859$) for $^{185}Re/^{187}Re$ values.

Results

Core sedimentology

Detailed descriptions of the lithofacies have been previously presented (Simms et al., 2022; Table S1). In brief, core LBA18-11R

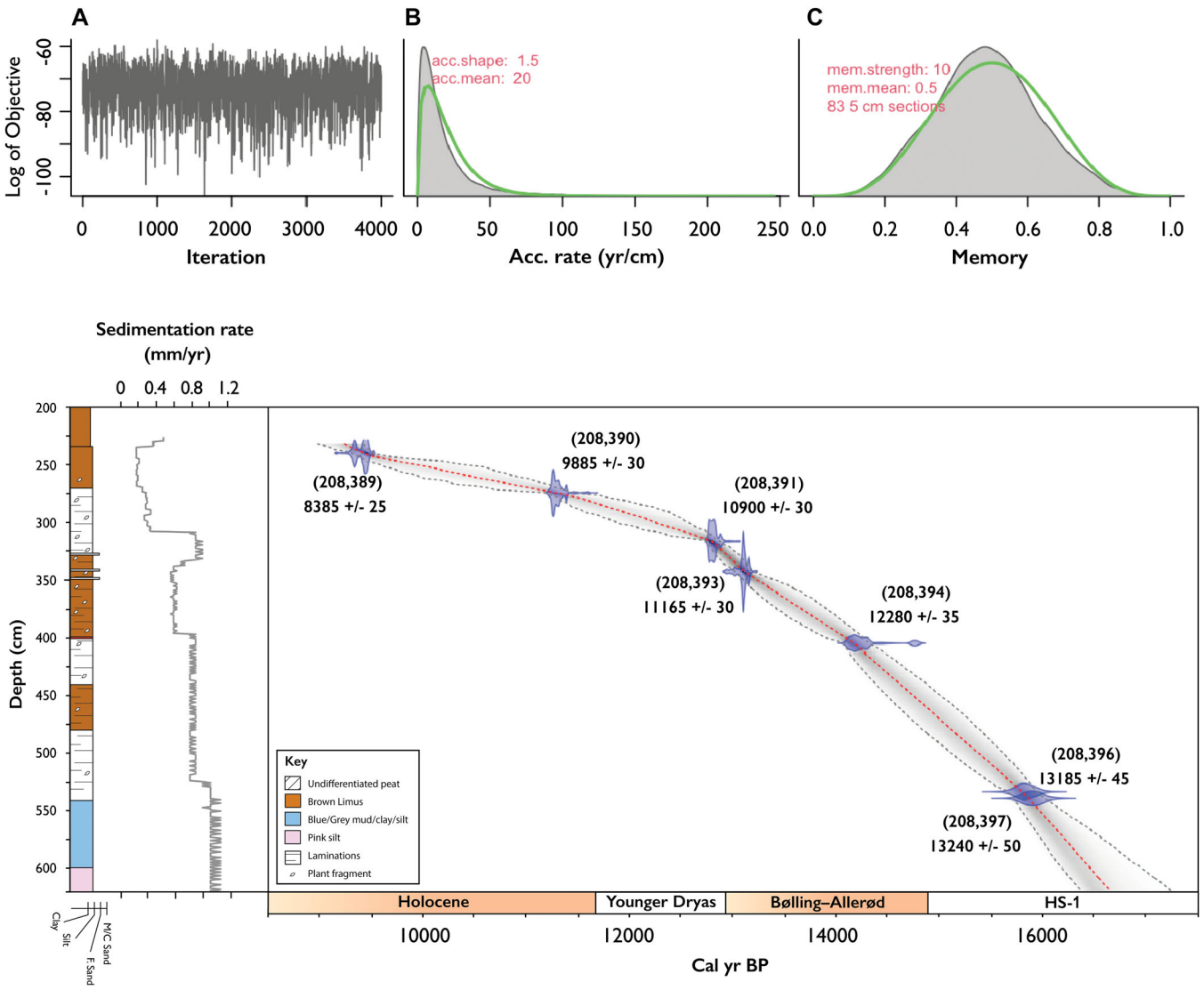

Figure 2. Age–depth model for the LBA18-11R core using the BACON (Blaauw and Christen, 2011) package (version 3.3.0) in R (version 4.4.1). The age–depth model shows calibrated ^{14}C ages depicted in blue, with the most accurate age model presented by a red dotted line (see text for discussion). The grey stippled lines indicate 95% confidence intervals. Calculated sedimentation rates are depicted on the adjacent plot. Plot (A) depicts iteration history, whereas plots (B) and (C) show prior, depicted by green lines, and posterior, shown by grey histograms, distributions for accumulation rate (B) and memory (C). The radiocarbon ages of each sample are shown in bold. [Color figure can be viewed at wileyonlinelibrary.com]

is 630 cm in length; pink silty clay is recorded from the core's base to 599 cm before a transition to blue–grey silty clay until 537 cm (Fig. 3). Between 537 and 477 cm, the sequence records slightly laminated grey silty clay with traces of sand. From 477 to 441 cm, limus with herbaceous fragments lies below an overlying laminated grey silty clay (441–398 cm). A 4 cm bed of red–brown silt overlies this unit (398–402 cm). Upsection, alternating units of limus and grey silty clay are preserved. Finally, above this, herbaceous peat is recorded (Fig. 3). The contacts between lithofacies appear gradational, with no clear erosive contacts identified within the stratigraphy.

Age modelling

The age–depth model developed here extrapolates a basal age of ~16.7 ka, suggesting that core LBA18-11R records sedimentation from the Late Glacial, with the age model spanning ~7500 years (Fig. 2). The sedimentation covers several significant events, including the Late Glacial, the Bølling-Allerød, the Older and Younger Dryas and the transition to the Holocene. Here, we use the traditional nomenclature for the time period since deglaciation common in the literature, noting that the Younger Dryas is equivalent to Greenland Stadial 1 (GS-1) and the Bølling-Allerød is equivalent to Greenland Interstadial 1 (GI-1) (Björck et al., 1998).

Character of wt% C, wt% N, $\delta^{13}C_{org}$ and C/N

The abundance of both carbon and nitrogen increases gradually between 630 and 480 cm from 0.05 to 2.02% and from 0.01 to 0.2%, respectively (Fig. 4; Table 1). Overall, concentrations vary broadly, with shifts coinciding with changes in lithology. Generally, the limnic units record higher carbon and nitrogen concentrations with peaks in both at 450 cm of 6.40 and 0.51%, respectively, whilst the silty clay units record lower values with dips in both recorded at 430 cm of 1.48 and 0.13%, respectively. Between 310 and 270 cm, a decrease in carbon concentration is observed, with values decreasing to 1.63% at 300 cm before increasing to 3.96% at 270 cm. The concentration of nitrogen follows a similar pattern, with a peak of 0.39% at 320 cm before a decrease to 0.10% at 290 cm.

Between 630 and 610 cm, $\delta^{13}C_{org}$ values remain constant between −27.30‰ and −27.15‰ (Fig. 4; Table 1). Upsection, there is a broad peak between 590 and 530 cm, with values reaching −20.05‰ at 560 cm before decreasing to −24.02‰ at

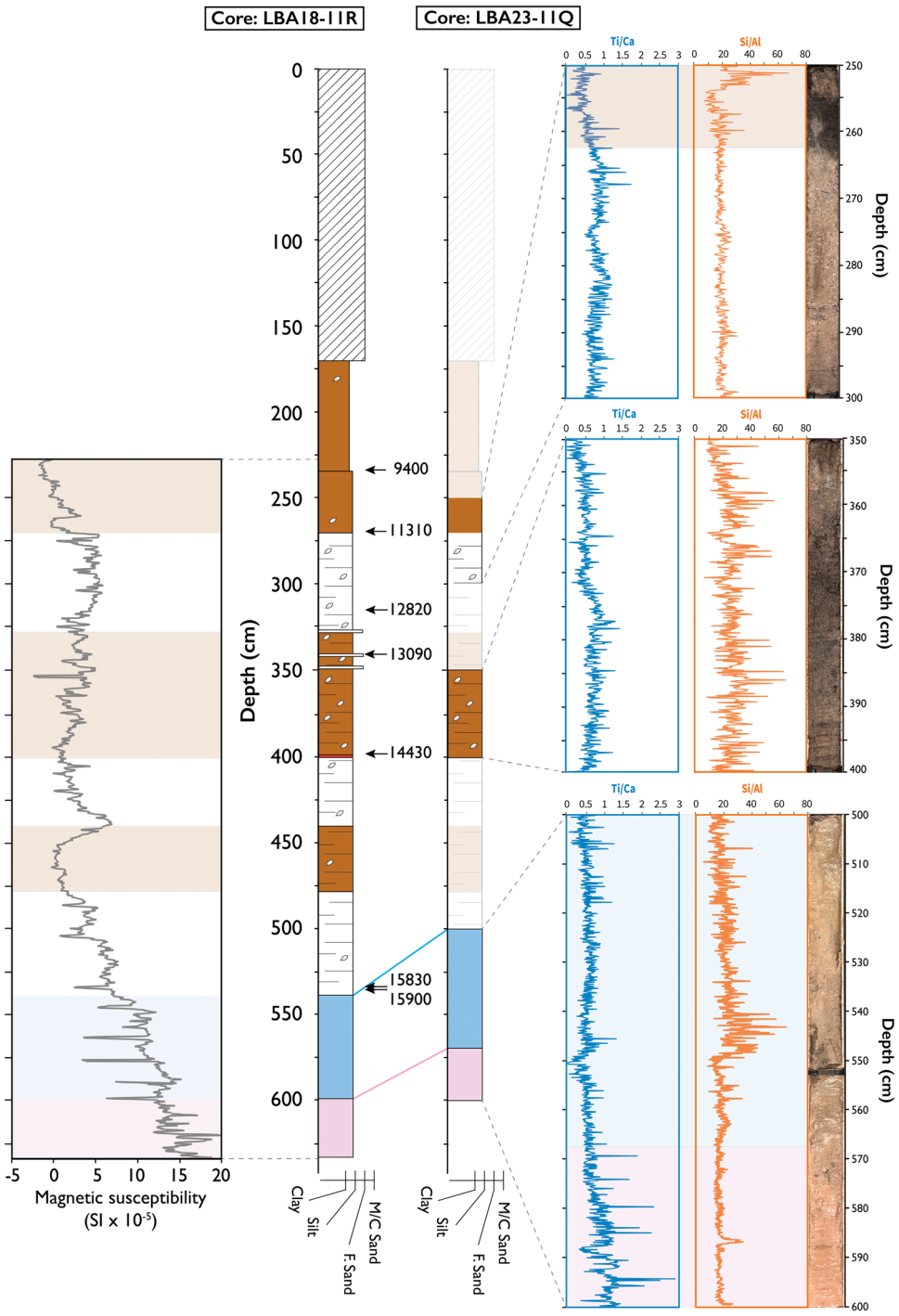

Figure 3. XRF scans for Ti/Ca and Si/Al with adjacent line scan images presented for LBA23-11Q core sections 250–300, 350–400, 500–550 and 550–600 cm. A stratigraphic log of LBA23-11Q is shown, with inferred lithologies denoted by paler colours. Adjacent is a stratigraphic log of core LBA18-11R. Correlations between the core sections and the stratigraphy are denoted by dashed lines. Core lithostratigraphy of LBA18-11R, median radiocarbon ages and magnetic susceptibility from Simms et al. (2022) are also presented. [Color figure can be viewed at wileyonlinelibrary.com]

530 cm and remaining similar until 450 cm. A second broad peak in $\delta^{13}C_{org}$ values is recorded between 410 and 370 cm, up to −20.76‰, before a subsequent broad decrease in values reaching −28.35‰ at 320 cm. The C/N values increase steadily upsection from 3.87 at the core's base to 17.14 at 270 cm, with a peak in values observed at 320 cm of 25.43 (Fig. 4; Table 1).

Re and Os abundance and Os-isotope composition

Rhenium abundance is similar between the core base and 610 cm (0.19–0.24 ppb), then rises sharply to 1.15 ppb at 590 cm, before declining to 0.25 ppb at 540 cm. Above this, values remain constant, with a broad peak of up to 0.60 ppb between 480 and 350 cm and a brief peak at 320 cm (0.48 ppb). The remainder of the core shows relatively consistent values (0.17 to 0.30 ppb). The total Os abundance ranges from 17.23 to 66.84 ppt, increasing from 19.28 ppt at the base to 33.01 ppt at 490 cm, with a broad maximum (up to 66.84 ppt) between 480 and 380 cm and two smaller peaks at 320 to 300 cm and 260 cm (Fig. 4; Table 1).

Given the age of the analysed sediment (ca. ≤17 kyrs) and relatively low Re abundance, any age correction for the post-depositional radiogenic ^{187}Os ingrowth from ^{187}Re decay would be less than that of the individual sample $^{187}Os/^{188}Os$ 2SE uncertainty (Table 1); therefore, age-corrected $^{187}Os/^{188}Os$

Table 1. Synopsis of wt% C, wt% N, $\delta^{13}C_{org}$ VPDB, C/N, Re and Os isotopic data, Loch Bad na h-Achlaise, Scotland.

Depth (cm)	C wt%	N wt%	δ^{13}C VPDB per mil	C/N	Re (ppb)	±*	Os_T (ppt)	±*	^{192}Os (ppt)	±*	^{187}Re/^{188}Os	±*	^{187}Os/^{188}Os	±*	rho	% Re blank	% ^{187}Os blank	% ^{188}Os blank
230					0.17	0.01	22.00	0.19	7.89	0.10	42.06	3.10	1.28	0.02	0.15	17.95	0.10	0.51
240					0.21	0.01	22.46	0.20	7.87	0.10	52.37	3.14	1.49	0.02	0.18	14.44	0.09	0.51
250					0.24	0.01	21.63	0.19	7.72	0.10	61.37	3.25	1.33	0.02	0.21	12.59	0.10	0.52
260					0.30	0.01	56.15	0.30	19.07	0.09	175.56	1.31	2.10	0.01	0.48	0.89	0.01	0.10
270	3.96	0.23	−19.54	17.14	0.20	0.03	26.89	0.23	9.12	0.11	698.69	10.56	1.79	0.03	0.66	0.93	0.06	0.44
280					0.22	0.01	19.00	0.17	6.73	0.10	65.23	3.72	1.39	0.02	0.22	13.56	0.11	0.60
290	1.73	0.10	−24.23	17.12	0.20	0.01	22.30	0.20	7.74	0.10	51.40	3.19	1.58	0.02	0.18	14.98	0.08	0.52
300	1.63	0.10	−26.32	17.02	0.20	0.01	32.82	0.17	11.78	0.07	286.08	2.30	1.28	0.01	0.54	0.89	0.03	0.17
310	3.41	0.19	−27.85	18.15	0.28	0.01	33.53	0.18	11.74	0.07	47.19	1.07	1.50	0.01	0.19	5.38	0.03	0.17
320	10.02	0.39	−28.35	25.43	0.48	0.01	38.69	0.22	13.13	0.07	224.37	1.84	1.79	0.01	0.50	1.01	0.02	0.15
340					0.20	0.01	22.20	0.59	7.57	0.38	445.23	22.66	1.75	0.13	0.67	0.89	0.04	0.27
350	2.43	0.16	−24.87	15.50	0.15	0.01	26.25	0.16	8.84	0.06	33.29	1.38	1.86	0.01	0.12	10.14	0.03	0.23
370	2.93	0.22	−20.96	13.31														
380					0.30	0.01	29.16	0.17	9.71	0.06	346.89	2.88	1.96	0.01	0.58	0.89	0.03	0.21
400					0.46	0.01	48.24	0.40	15.76	0.15	58.27	1.70	2.15	0.03	0.25	6.49	0.03	0.25
410	4.40	0.32	−20.76	13.88														
425					0.30	0.01	56.47	0.32	18.31	0.09	183.94	1.38	2.22	0.01	0.48	0.89	0.01	0.11
430	1.48	0.13	−25.22	11.54														
450	6.40	0.51	−23.33	12.56														
460					0.60	0.01	66.84	0.46	21.77	0.12	170.21	1.37	2.18	0.02	0.42	0.89	0.01	0.10
480	2.02	0.20	−24.03	10.22	0.40	0.01	42.48	0.25	13.64	0.07	247.07	1.92	2.32	0.02	0.52	0.89	0.02	0.15
490	1.59	0.16	−24.26	9.74	0.20	0.01	33.01	0.19	10.97	0.06	307.23	2.48	1.99	0.01	0.56	0.89	0.02	0.18
510	1.01	0.11	−23.20	8.89	0.20	0.01	31.53	0.18	10.50	0.06	320.94	2.61	1.96	0.01	0.57	0.89	0.02	0.19
525					0.22	0.01	35.52	0.20	11.82	0.07	37.79	1.05	1.97	0.01	0.16	6.68	0.02	0.17
530	0.76	0.09	−24.02	8.10														
540	0.77	0.09	−22.94	8.43	0.25	0.01	31.70	0.19	10.44	0.06	47.95	1.20	2.07	0.02	0.19	5.96	0.02	0.19
543					0.31	0.01	34.21	0.19	11.81	0.07	51.69	1.08	1.63	0.01	0.21	4.89	0.03	0.17
547					0.43	0.01	23.45	0.13	8.21	0.05	103.66	1.67	1.50	0.01	0.34	3.50	0.04	0.24
550	0.18	0.03	−21.56	6.26	0.30	0.01	23.96	0.13	8.44	0.06	70.47	1.52	1.45	0.01	0.25	5.01	0.04	0.24
560	0.18	0.03	−20.05	6.32	0.70	0.01	26.72	0.14	9.60	0.06	351.25	2.92	1.27	0.01	0.59	0.89	0.04	0.21
570	0.16	0.02	−21.74	7.10														
575					0.85	0.01	24.89	0.11	8.97	0.05	188.28	1.73	1.24	0.01	0.49	1.77	0.04	0.22
590	0.15	0.02	−20.32	6.08	1.15	0.02	22.00	0.19	7.89	0.10	422.50	7.22	1.29	0.02	0.64	1.79	0.10	0.51
600					0.60	0.01	17.23	0.11	6.13	0.05	549.48	5.37	1.35	0.01	0.69	0.89	0.06	0.33
610	0.05	0.02	−27.30	2.91	0.24	0.01	25.32	0.14	9.02	0.06	53.26	1.39	1.34	0.01	0.20	6.21	0.04	0.22
620					0.19	0.01	30.76	0.16	10.99	0.06	34.07	1.11	1.32	0.01	0.14	7.97	0.03	0.18
630	0.05	0.01	−27.15	3.87	0.20	0.01	19.28	0.11	6.86	0.05	491.56	4.57	1.36	0.01	0.67	0.89	0.05	0.29

*All uncertainties are 2σ absolute.

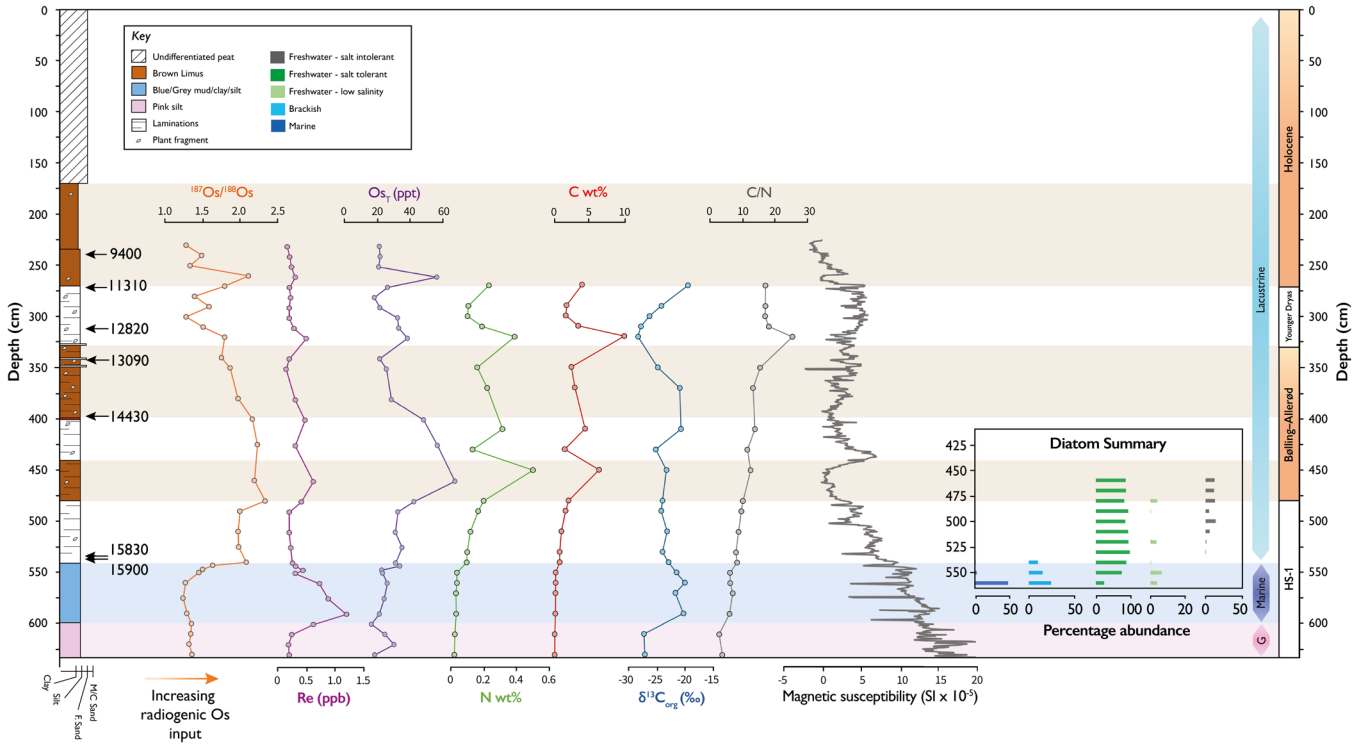

Figure 4. Proxy comparison for LBA18-11R, including $^{187}Os/^{188}Os$, Re (p.p.b.), OsT (total p.p.t.), wt% N, wt% C, $\delta^{13}C_{org}$ (‰) and C/N. Core lithostratigraphy, median radiocarbon ages, magnetic susceptibility and a diatom summary from Simms et al. (2022) are also presented. The pink shaded region indicates a glaciomarine (G) depositional setting. [Color figure can be viewed at wileyonlinelibrary.com]

values are not presented. Throughout the core, the $^{187}Os/^{188}Os$ values range from 1.24 to 2.32 (Fig. 4; Table 1). Between 630 and 600 cm, $^{187}Os/^{188}Os$ values range between 1.32 and 1.36, before decreasing slightly to 1.24 at 575 cm. Upsection, a significant increase in $^{187}Os/^{188}Os$ values is observed, with values reaching 2.07 at 540 cm (Fig. 4; Table 1). The $^{187}Os/^{188}Os$ values remain elevated until 320 cm, ranging from 1.75 to 2.32. Between 320 and 260 cm, there is a significant decrease in $^{187}Os/^{188}Os$ values to 1.28 at 300 cm. Finally, a subsequent peak in $^{187}Os/^{188}Os$ values is recorded at 260 cm (2.10), before a gradual decrease to 1.28 at 230 cm.

XRF

We focus on Ti/Ca (Fig. 3), a proxy for sediment sources: Ti reflects terrigenous siliciclastic input, whilst Ca indicates marine biogenic carbonate. This ratio is widely used to reconstruct terrigenous input (Nace et al., 2014; Gregory et al., 2015; Rothwell and Croudace, 2015; Hou et al., 2020). We also examine Si/Al, which reflects the relative contributions of quartz, which contains abundant Si, to clay, which is rich in Al (Tisserand et al., 2009; Sano et al., 2013; Clift et al., 2014). The XRF results will be described with respect to each section of core LBA23-11Q.

500–600 cm: Between 600 and 580 cm, Ti/Ca values are elevated (~1.2), whilst upsection values decrease to ~0.5 (Fig. 3; Table S3.1). Si/Al values are relatively stable, averaging ~15 between 600 and 548 cm, before increasing slightly to ~25 on average between 548 and 500 cm.

350–400 cm: Ti/Ca values remain relatively stable (~0.8) between 400 and 370 cm, before decreasing marginally to 0.5 upsection (Fig. 3; Table S3.2). Similarly, Si/Al values remain relatively stable, averaging ~25 throughout this core section.

250–300 cm: Ti/Ca values remain relatively stable at ~1 between 300 and 262 cm, before a slight decrease to ~0.4 (Fig. 3; Table S3.3). Between 300 and 262 cm, Si/Al values remain stable at ~20; upsection values increase gradually, with a brief peak in values in the uppermost 3 cm of the core with values of up to ~60.

Discussion

The discussion of the proxy data of this study to understand the palaeoenvironment of this site will be presented from the basal section upwards. We then review the usefulness of osmium isotopes for palaeoenvironmental reconstruction and the implications of our new data for the RSL changes in this region.

Glacial (16.7–16.5 cal ka BP)

Samples from this period plot close to the freshwater particulate organic carbon (POC) field of the $\delta^{13}C_{org}$ versus C/N ratio biplot, suggesting that freshwater inputs dominated the carbon pool (Fig. 5; Lamb et al., 2006). The high magnetic susceptibility values and elevated Ti/Ca values (Figs. 3 and 4; Table S3.1) recorded between 16.7 and 16.5 cal ka BP indicate increased terrestrial input (e.g., Diekmann et al., 2000; Bahr et al., 2005; Van Hoang et al., 2010; Kim et al., 2022) into the basin. These data are supportive of a glacial environment at this time, as suggested by the sedimentology (Simms et al., 2022), with the freshwater being derived from meltwater supplied to the basin from the local retreating BIIS.

While these traditional methods reconstruct a glacial setting, this period lacks any biostratigraphic framework, which hampers palaeoenvironmental reconstruction. Here, the $^{187}Os/^{188}Os$ record is particularly suited to further investigate the nature of the depositional environment. The $^{187}Os/^{188}Os$ data from Late Glacial marine sediments at Loch Duart (70 km north of Gairloch) provide the best estimate of the $^{187}Os/^{188}Os$ composition of seawater in this region at approximately this time (Taylor et al., 2024). That study yielded ~1.06 during marine deposition, which agrees with the

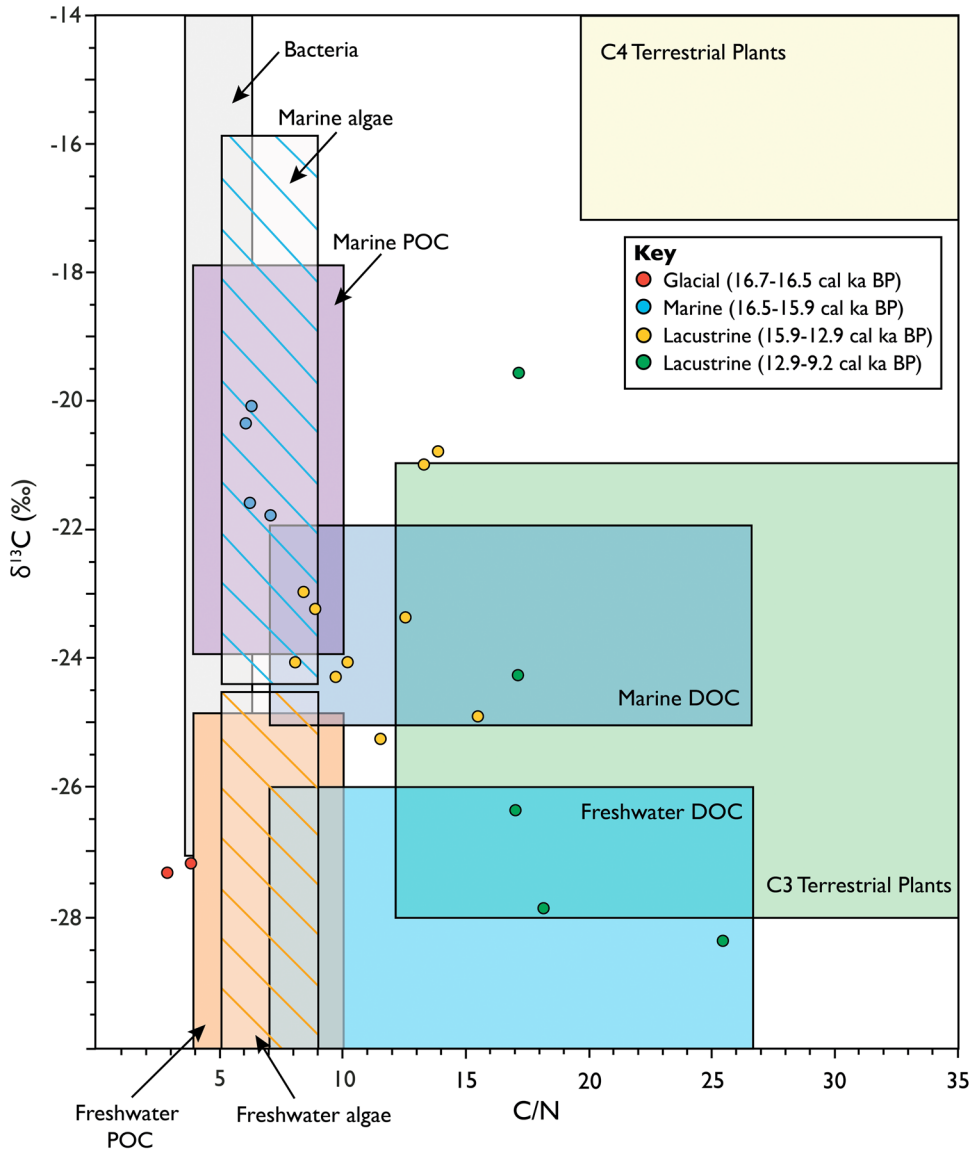

Figure 5. C/N and $\delta^{13}C$ from bulk organic material from core LBA18-11R. The fields of organic inputs to coastal environments are based on typical ranges of $\delta^{13}C$ and C/N ranges detailed in Lamb et al. (2006). [Color figure can be viewed at wileyonlinelibrary.com]

$^{187}Os/^{188}Os$ signature of open seawater ~1.04–1.06 (e.g., Sharma et al., 1997; Levasseur et al., 1998; Peucker-Ehrenbrink and Ravizza, 2000; Gannoun and Burton, 2014; Rooney et al., 2016). Therefore, the elevated $^{187}Os/^{188}Os$ values (1.32–1.36) of the basal pink silty clay at Loch Bad na h-Achlaise above marine values suggest an increased input of radiogenic sources of Os. This is interpreted to represent increased weathering of the surrounding bedrock and enhanced delivery of weathered material to the basin through meltwater associated with the retreat of the BIIS. Although the $^{187}Os/^{188}Os$ values over this section are higher than that of present-day seawater, they are relatively low compared to other sections in the core (Section 5.3), suggesting that the basin was not fully isolated from marine influence. Thus, the $^{187}Os/^{188}Os$ record supports the palaeoenvironmental interpretation of the traditional proxy data set, indicating that between 16.7 and 16.5 cal ka BP, the basin was dominated by glacial meltwater delivering glacially eroded terrestrial material from a proximal retreating glacier.

Marine (16.5–15.9 cal ka BP)

Throughout this section, carbon and nitrogen concentrations are similar to those of the underlying unit, indicating continued low productivity. The increase in C/N and $\delta^{13}C_{org}$ values over this period means that samples plot within the marine algae and marine POC fields in $\delta^{13}C_{org}$ versus C/N space, which is in agreement with the diatom interpretation of brackish and marine conditions (Fig. 5; Simms et al., 2022). The marginal increase in Si/Al suggests a potential reduction in the contribution of clay within this section. A slight decrease in Ti/Ca values is also recorded within this section (Fig. 3; Table S3.1). This is likely due to a combination of dilution from the marine water column and a reduction in terrestrial input to the basin as glacial meltwater flux was reduced by retreating glaciers in the catchment.

Once more, the traditional proxies applied here concur and broadly imply a marine depositional setting; however, the application of the $^{187}Os/^{188}Os$ system reveals further insights into the dynamics of the basin and RSL over this period. The slight decrease in $^{187}Os/^{188}Os$ values compared with the underlying glacial unit may suggests a marginal reduction in the input of radiogenic Os. This reduction is likely due to a decrease in the input of glacially eroded catchment bedrock because the retreat of the local ice sheet allowed a relative increase in the input of marine sourced Os through connection to the open ocean (Fig. 6). Upsection, the increase in $^{187}Os/^{188}Os$ values (up to 1.63 at 543 cm) coincides with the

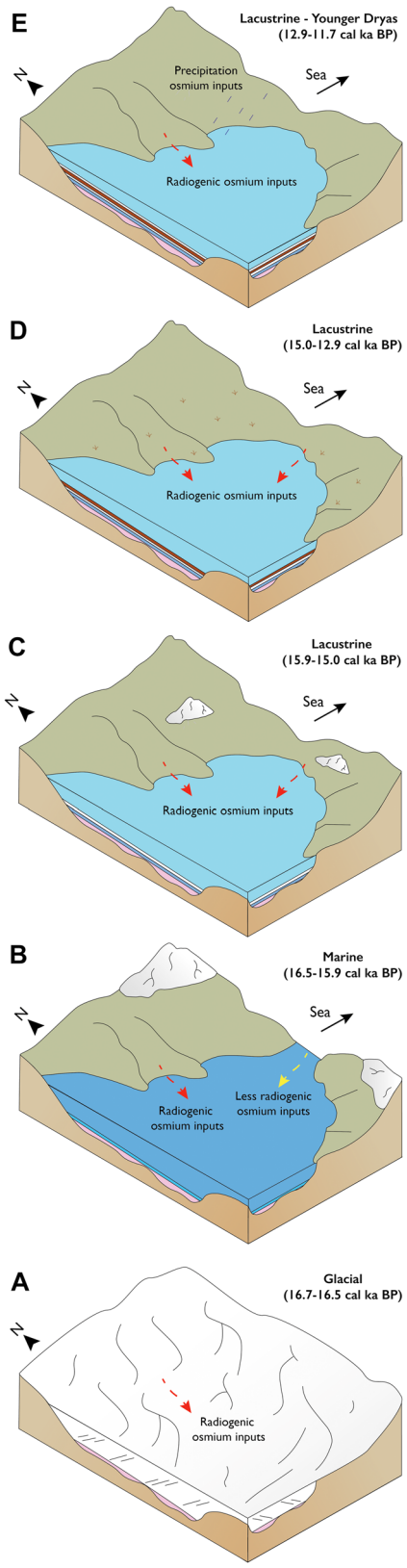

Figure 6. Block diagrams showing the palaeoenvironment evolution of Loch Bad na h-Achlaise from the Late Glacial to the Holocene. See text for discussion. [Color figure can be viewed at wileyonlinelibrary.com]

increase in freshwater diatom species (Simms et al., 2022); it thus records the gradual isolation of the basin and therefore the increased influence of terrestrially derived Os. This interpretation is further supported by a significant increase in Re abundance, before it subsequently decreases upsection as the basin gradually becomes isolated (Fig. 4; Table 1). Rhenium is known to covary with salinity and displays conservative behaviour in oxic waters (Anbar et al., 1992; Colodner et al., 1993). The increase–decrease trend in Re over this period suggests a similar increase–decrease trend in the salinity of the basin, which is consistent with the transition from a glaciomarine to a marine depositional setting, followed by basin isolation. The Os and Re records here reveal a more complex palaeoenvironmental history of the basin and RSL than implied by traditional proxies alone, highlighting the utility of applying more novel techniques to sedimentary archives.

Lacustrine (15.9–12.9 cal ka BP)

The pattern of carbon and nitrogen concentrations over this period is most likely due to greater productivity within and around the basin during relatively warm organic-rich limnic deposition and a reduction in basin productivity during the deposition of the grey silty clay during the cooler Older Dryas. Most of the samples from this section fall between the ranges of marine POC, marine dissolved organic carbon (DOC) and C3 terrestrial plants, which reflects a mixed organic carbon pool (Fig. 5). Whilst the samples vary within $\delta^{13}C_{org}$ versus C/N space over this period, the general shift to higher C/N ratios indicates a larger relative input of higher order plant material, suggesting a reduction in marine influence.

The most notable geochemical feature of this period is the increase in $^{187}Os/^{188}Os$ values towards the most radiogenic values within the core (2.32 at 480 cm), reflecting increased input of terrestrially derived osmium sourced from radiogenic bedrock and a relative decrease in unradiogenic contributions (Fig. 6). This shift is linked to the isolation of the basin isolation due to a fall in RSL. This is supported by microfossil evidence, as the most radiogenic $^{187}Os/^{188}Os$ values coincide with the appearance and increase in freshwater salt-intolerant diatom species (Simms et al., 2022), suggesting that by this time, the basin was fully isolated from tidal influence and dilution from less radiogenic osmium inputs from seawater. Concurrently, Re abundance declines to 0.25 ppb at 540 cm (Fig. 4; Table 1), which is consistent with the reduced salinity as the basin became isolated, given the generally conservative behaviour of rhenium with salinity.

Lacustrine–Younger Dryas to Holocene (12.9–9.2 cal ka BP)

At the beginning of this period, decreases in carbon and nitrogen concentrations are coincident with a lithological change from limus to silty clay, suggesting a reduction in basin productivity. This is most likely linked to the cooler climate conditions of the Younger Dryas. The increase in Si/Al values over the transition from Younger Dryas to Holocene likely also reflects a lithological change from slightly laminated grey silty clay and overlying limus and therefore a reduction in aluminosilicates (Fig. 3). The samples from this period plot largely within the freshwater DOC, C3 terrestrial plant and marine DOC fields, suggesting that the organic carbon pool is dominated by freshwater and terrestrial plant inputs (Fig. 5). The shift to the highest C/N ratios recorded in the core indicates a larger relative input of higher order plant material, typically terrestrial vegetation in the organic fraction.

While the traditional proxies applied here suggest a period of freshwater deposition, they do not resolve the nuanced changes in climate. This is further resolved in the $^{187}Os/^{188}Os$ record. The most notable geochemical feature of this period is the broad decrease in $^{187}Os/^{188}Os$ values coinciding with the cooler Younger Dryas. Whilst marine inundation into the basin

is one explanation for such a reduction in $^{187}Os/^{188}Os$ values, this is unlikely, based on the other proxies recorded and our knowledge of the regional sea-level history. Previous sea-level index points and GIA modelling at this site and the nearby sites of Assynt and Fearnbeg indicate that RSL was at or below present-day sea level (approximately −5 m; Shennan et al., 2018; Simms et al., 2022) at this time. Second, the other proxies presented here do not provide evidence of marine influence at this time. The abundance of Re remains very similar throughout the Younger Dryas and Early Holocene, suggesting no significant change in the salinity of the basin. Additionally, samples from this period plot in the freshwater rather than marine fields in $\delta^{13}C$ versus C/N space, also arguing against marine input (Fig. 5). We instead postulate that a reduction in the delivery of radiogenic osmium into the basin associated with a cooling climate allowed the $^{187}Os/^{188}Os$ signature of precipitation to dominate the signal, resulting in reduced $^{187}Os/^{188}Os$ values. Although modern precipitation $^{187}Os/^{188}Os$ values are affected by human-induced pollution, resulting in unradiogenic values of 0.16–0.48, with samples from Europe yielding 0.275, it is assumed that before significant anthropogenic influence, precipitation showed a $^{187}Os/^{188}Os$ signature of ~1.0, similar to that of the ocean (Chen et al., 2009). Additionally, studies have suggested that the southward shift of the oceanic polar front resulted in increased precipitation across western Scotland during the early Younger Dryas (Ruddiman and McIntyre, 1981; Bard et al., 1987; Isarin and Renssen, 1999; Ballantyne, 2002). Therefore, due to the lack of other evidence of a marine intrusion, we suggest that the reduction in $^{187}Os/^{188}Os$ values over this period is due to a reduction in the delivery of terrestrially sourced radiogenic osmium into the basin associated with the cooling climate of the onset of the Younger Dryas, with the Os isotope signature of the basin more likely recording increasing dominance of Os inputs through precipitation (Fig. 6). An increase in precipitation could also explain the subtle decrease in $^{187}Os/^{188}Os$ values from 2.15 to 1.79 between 14.2 cal ka BP and the onset of the Younger Dryas.

A brief return to more radiogenic $^{187}Os/^{188}Os$ values (2.10) is coincident with the end of the Younger Dryas before a decrease to 1.28 (230 cm). Based on mapped limits, the glaciers that advanced during the Younger Dryas do not appear to have advanced to Loch Bad na h-Achlaise but reached their limit nearby (Fig. 1; Bickerdike et al., 2018). Therefore, increased glacial meltwater input into the nearby catchment following the Younger Dryas may have delivered more radiogenic Os to the basin. Additionally, a reduction in vegetation cover during the Younger Dryas, coupled with greater precipitation, may have led to the temporary mobilisation of soils across the transition between the Younger Dryas and the Holocene. This could have also contributed to the more radiogenic $^{187}Os/^{188}Os$ values. Following this, increased vegetation cover as the climate warmed would act to protect terrestrial sediment from erosion, leading to a reduction in the delivery of radiogenic material and a corresponding decrease in $^{187}Os/^{188}Os$ values (~1.28) once more. This suggests that the Os isotope system could be used as an indirect measure of catchment erosion linked to climate and vegetation cover shifts.

New insights from the $^{187}Os/^{188}Os$ record

The application of the $^{187}Os/^{188}Os$ isotope system in an isolation basin setting has demonstrated the proxy to be a robust tracer of marine inundation and basin isolation. The $^{187}Os/^{188}Os$ record shows remarkable agreement with the traditional proxies applied and is sensitive to more nuanced changes in palaeoenvironment.

The basal pink silty clay shows elevated $^{187}Os/^{188}Os$ values (1.32–1.36), slightly higher than the marine seawater signature, reflecting glaciomarine deposition with enhanced input of radiogenic, glacially derived Os. The base of the overlying blue–grey marine silty clay records slightly lower values (1.24–1.29), indicating reduced radiogenic input and greater marine influence. The $^{187}Os/^{188}Os$ values subsequently increase to 1.63, signalling increased terrestrial Os input and diminished marine influence during RSL fall. This trend continues in the laminated grey silty clay, where values reach up to 2.32, marking a relative increase in continentally derived radiogenic osmium inputs and a reduction in the marine supply of unradiogenic sources of Os as the basin became isolated from the sea.

The subsequent reduction in $^{187}Os/^{188}Os$ values coincident with the Younger Dryas is interpreted to be due to a reduction in the delivery of terrestrially sourced radiogenic osmium associated with the cooling climate. The Os isotope signature of the basin therefore likely recorded the increasing dominance of Os inputs through increased precipitation across western Scotland during the early Younger Dryas (Ruddiman and McIntyre, 1981; Bard et al., 1987; Isarin and Renssen, 1999; Ballantyne, 2002).

A similar $^{187}Os/^{188}Os$ profile is observed over this period at Loch Sunart, with a reduction in values (1.12–1.16) between 12.9 and 11.7 cal ka BP (Taylor et al., 2025). Loch Sunart is a fjord, rather than an isolation basin, and as such, the inflow of saline waters from offshore as the local ice sheet retreated may have contributed to the lowering of $^{187}Os/^{188}Os$ values at this site. However, a reduction in the delivery of radiogenic osmium into the basin associated with BIIS readvance and an increase in the relative influence of precipitation on the osmium isotope signature have been postulated as a possible additional mechanism, as suggested here for Loch Bad na h-Achlaise.

This reduction in $^{187}Os/^{188}Os$ values during the Younger Dryas has been identified at another isolation basin (Loch Duart, Taylor et al., 2024). As with the Loch Bad na h-Achlaise site of this study, Loch Duart has been shown to be isolated through the Younger Dryas (Hamilton et al., 2015; Taylor et al., 2024; Podrecca et al., 2025); hence, the less radiogenic Os signal most likely reflects the increased influence of precipitation. Further work at a greater number of sites is needed to investigate this trend. However, the presence of a decrease in $^{187}Os/^{188}Os$ values at a similar time at Loch Duart, Loch Sunart and in this study during the Younger Dryas suggests that the $^{187}Os/^{188}Os$ isotope system has the potential for use for identification of changes in climatic conditions as well as RSL history.

This history of basin isolation is clearly recorded in the $^{187}Os/^{188}Os$ record, from glaciomarine to marine deposition, with the subsequent freshwater phase possessing a markedly more radiogenic signature. This record highlights the utility of this novel method, which is not reliant on microfossil preservation, as a tracer of RSL fall and subsequent basin isolation. Additionally, this study's multiproxy approach highlights the merit of applying a varied geochemical toolkit to a sedimentary archive, as it allows more nuanced and robust interpretations and increases the overall reliability of palaeoenvironmental reconstructions.

New insights into relative sea-level change at Loch Bad na h-Achlaise

Comparison of this $^{187}Os/^{188}Os$ record with the established biostratigraphic framework based on diatom species shows that the Os isotope system can reliably track the transition from

marine inundation to basin isolation associated with relative sea-level change. The $^{187}Os/^{188}Os$ record can also be utilised to identify changes in basin and catchment processes linked to erosion and delivery of radiogenic material to the basin. Additionally, the isotope system can be used to assess RSL changes in sections with poor or no diatom preservation, for example, the basal pink silt at Loch Bad na h-Achlaise. The relatively unradiogenic Os values through the lower pink silt indicate that this is glaciomarine in origin. This indicates a significant period of marine inundation of the basin following deglaciation, initially in a glaciomarine environment, then over the transition to blue–grey silty clay in a marine environment as ice retreated from the basin catchment. The initiation of isolation is then identified by the gradual increase in Os isotopic values.

The marine limit at Gairloch has not been directly dated but was previously estimated to be 16.3 ± 0.2 ka by Simms et al. (2022) using the rate of RSL fall from the Kuchar et al. (2012) GIA model in conjunction with the difference in elevation between the Loch Bad na h-Achlaise RSL indicators and the elevation of the local marine limit. The $^{187}Os/^{188}Os$ record presented here shows consistent values across the marine interval until 560 cm, where values begin to increase, implying greater input of radiogenic material and therefore RSL fall. This, combined with the robust age model, provides a minimum age of the marine limit at this site and constrains the initiation of RSL fall to 16.2 cal ka BP. This age is in close agreement and within uncertainty of the previous age estimate of the marine limit at this site. Using the 16.2-ka age estimate of this study for the marine limiting point, alongside the RSL observations of Simms et al. (2022), we calculate a rate of RSL change of ~22 mm/yr, which is comparable to the rates estimated from the Kuchar et al. (2012) model at this time. This indicates that the Os isotope system can not only identify RSL changes, but when combined with an age–depth model, can also be used to determine the rates of such changes and the minimum ages of marine limits.

Implications and Conclusions

- The osmium isotope record highlights glaciomarine conditions during deposition of a basal glacial unit with elevated $^{187}Os/^{188}Os$ values, suggesting enhanced ice-sheet weathering of the surrounding bedrock. The glaciomarine setting was previously unresolved due to the absence of a biostratigraphic framework. This demonstrates the merit of the Os isotope system for sites with limited or no preservation of microfossils during deglacial periods, which often hampers palaeoenvironmental reconstructions (e.g., Shemesh et al., 1989; Bradbury et al., 1994; Fang et al., 2024).
- Distinct $^{187}Os/^{188}Os$ values at this site effectively differentiate periods of marine influence (~1.2) from isolated conditions (>2.0), allowing the reconstruction of a complex RSL history.
- The $^{187}Os/^{188}Os$ record, combined with the robust age model, provides a minimum age of the marine limit and the onset of RSL fall (16.2 cal ka BP). Using this age, we calculate a rate of RSL fall of ~22 mm/yr, which is comparable to GIA model estimates for the region (e.g., Kuchar et al., 2012).
- During the Younger Dryas, the osmium isotope profile at Loch Bad na h-Achlaise shows a decline in $^{187}Os/^{188}Os$ values that is unlikely to reflect a marine intrusion, given regional sea level at this time and the elevation of the basin's sill. Instead, colder conditions likely reduced erosion and therefore radiogenic osmium input, allowing the osmium isotope composition of precipitation to dominate rather than radiogenic weathered bedrock. This trend parallels records from Loch Duart and Loch Sunart, indicating that lower $^{187}Os/^{188}Os$ values over this period record the regional effect of the Younger Dryas. Thus, the Os isotope profiles of isolation basins and fjord settings could serve as an indirect measure of catchment erosion linked to changes in climate and vegetation cover.
- Future applications of Os isotopes could address broader questions regarding the spatial variability of RSL change and the timing of glacial retreat. By extending this approach across multiple basins, future work could test the regional coherence of the Younger Dryas signature and refine GIA models with independent RSL constraints. Moreover, integration of Os isotopes with traditional proxies may further elucidate the relative roles of climate, vegetation and hydrology in shaping erosion and sediment delivery. This method offers new opportunities to reconstruct palaeoenvironments in settings and over time periods where conventional microfossil records are incomplete or absent.

Acknowledgements. We thank Neil Tunstall and Chris Longley for their analytical support and the use of the Geotek X-ray core imaging system (MSCL-XCT) within the Department of Geography at Durham University (UK). We also acknowledge the support of Chris Ottley and Geoff Nowell and the use of the Durham Geochemistry Centre within the Department of Earth Sciences at Durham University. We thank Trap Puckette for his analytical support and Ian Shennan for inspiring this work and help with collection of the core. This work benefited from discussions during the 2023 QRA Wester Ross Field Meeting. This study was funded by the Durham Doctoral Scholarship of Durham University. ARS was funded by the NSFGEO-NERC Grant #2147750. LB was funded by the NERC grant NE/X009343/1.

Conflicts of Interest—The authors declare no conflicts of interest.

Data Availability Statement

The authors confirm that the data supporting the findings of this study are available within the article and its supplementary materials.

Supporting information

Additional supporting information can be found in the online version of this article.

supplementary_information.

References

Anbar, A.D., Creaser, R.A., Papanastassiou, D.A. & Wasserburg, G.J. (1992) Rhenium in seawater: Confirmation of generally conservative behavior. *Geochimica et Cosmochimica Acta*, 56(11), 4099–4103. Available from: https://doi.org/10.1016/0016-7037(92)90021-A

Bahr, A., Lamy, F., Arz, H., Kuhlmann, H. & Wefer, G. (2005) Late glacial to Holocene climate and sedimentation history in the NW Black Sea. *Marine Geology*, 214(4), 309–322. Available from: https://doi.org/10.1016/j.margeo.2004.11.013

Ballantyne, C.K. (2002) The Loch Lomond Readvance on the Isle of Mull, Scotland: Glacier reconstruction and palaeoclimatic implications. *Journal of Quaternary Science*, 17(8), 759–771. Available from: https://doi.org/10.1002/jqs.729

Bard, E., Arnold, M., Maurice, P., Duprat, J., Moyes, J. & Duplessy, J.-C. (1987) Retreat velocity of the North Atlantic polar front during the last deglaciation determined by 14C accelerator mass spectrometry. *Nature*, 328(6133), 791–794. Available from: https://doi.org/10.1038/328791a0

Best, L. & Shennan, I. (2024) Scottish landform example: isolation basins of Arisaig. *Scottish Geographical Journal*, 141, 1–20. Available from: https://doi.org/10.1080/14702541.2024.2401166

Best, L., Simms, A.R., Brader, M., Lloyd, J., Sefton, J. & Shennan, I. (2022) Local and regional constraints on relative sea-level changes in southern Isle of Skye, Scotland, since the Last Glacial Maximum. *Journal of Quaternary Science*, 37(1), 59–70. Available from: https://doi.org/10.1002/jqs.3376

Bickerdike, H.L., Evans, D.J.A., Stokes, C.R. & Ó Cofaigh, C. (2018) The glacial geomorphology of the Loch Lomond (Younger Dryas) Stadial in Britain: a review. *Journal of Quaternary Science*, 33(1), 1–54. Available from: https://doi.org/10.1002/jqs.3010

Björck, S., Walker, M.J.C., Cwynar, L.C., Johnsen, S., Knudsen, K.L., Lowe, J.J. et al. (1998) An event stratigraphy for the last termination in the North Atlantic region based on the Greenland ice-core record: a proposal by the INTIMATE group. *Journal of Quaternary Science*, 13(4), 283–292. Available from: https://doi.org/10.1002/(SICI)1099-1417(199807/08)13:4<283::AID-JQS386>3.0.CO;2-A

Blaauw, M. & Christen, J.A. (2011) Flexible paleoclimate age-depth models using an autoregressive gamma process. *Bayesian Analysis*, 6(3), 457–474. Available from: https://doi.org/10.1214/11-BA618

Bradbury, J.P., Bezrukova, Y.V., Chernyaeva, G.P., Colman, S.M., Khursevich, G., King, J.W. et al. (1994) A synthesis of post-glacial diatom records from Lake Baikal. *Journal of Paleolimnology*, 10, 213–252.

Bradley, S.L., Milne, G.A., Shennan, I. & Edwards, R. (2011) An improved glacial isostatic adjustment model for the British Isles. *Journal of Quaternary Science*, 26(5), 541–552. Available from: https://doi.org/10.1002/jqs.1481

Bradwell, T., Fabel, D., Clark, C.D., Chiverrell, R.C., Small, D., Smedley, R.K. et al. (2021) Pattern, style and timing of British–Irish Ice Sheet advance and retreat over the last 45 000 years: evidence from NW Scotland and the adjacent continental shelf. *Journal of Quaternary Science*, 36(5), 871–933. Available from: https://doi.org/10.1002/jqs.3296

Bradwell, T., Small, D., Fabel, D., Smedley, R.K., Clark, C.D., Saher, M.H. et al. (2019) Ice-stream demise dynamically conditioned by trough shape and bed strength. *Science Advances*, 5(4), eaau1380. Available from: https://doi.org/10.1126/sciadv.aau1380

Chen, C., Sedwick, P.N. & Sharma, M. (2009) Anthropogenic osmium in rain and snow reveals global-scale atmospheric contamination. *Proceedings of the National Academy of Sciences*, 106(19), 7724–7728. Available from: https://doi.org/10.1073/pnas.0811803106

Clark, C.D., Ely, J.C., Hindmarsh, R.C.A., Bradley, S., Ignéczi, A., Fabel, D. et al. (2022) Growth and retreat of the last British–Irish Ice Sheet, 31 000 to 15 000 years ago: the BRITICE-CHRONO reconstruction. *Boreas*, 51(4), 699–758. Available from: https://doi.org/10.1111/bor.12594

Clark, C.D., Hughes, A.L.C., Greenwood, S.L., Jordan, C. & Sejrup, H.P. (2012) Pattern and timing of retreat of the last British-Irish Ice Sheet. *Quaternary Science Reviews*, 44, 112–146. Available from: https://doi.org/10.1016/j.quascirev.2010.07.019

Clift, P.D., Wan, S. & Blusztajn, J. (2014) Reconstructing chemical weathering, physical erosion and monsoon intensity since 25Ma in the northern South China Sea: a review of competing proxies. *Earth-Science Reviews*, 130, 86–102. Available from: https://doi.org/10.1016/j.earscirev.2014.01.002

Cohen, A.S., Coe, A.L., Bartlett, J.M. & Hawkesworth, C.J. (1999) Precise Re-Os ages of organic-rich mudrocks and the Os isotope composition of Jurassic seawater. *Earth and Planetary Science Letters*, 167, 159–173.

Colodner, D., Sachs, J., Ravizza, G., Turekian, K., Edmond, J. & Boyle, E. (1993) The geochemical cycle of rhenium: a reconnaissance. *Earth and Planetary Science Letters*, 117, 205–221.

Diekmann, B., Kuhn, G., Rachold, V., Abelmann, A., Brathauer, U., Fütterer, D.K. et al. (2000) Terrigenous sediment supply in the Scotia Sea (Southern Ocean): response to Late Quaternary ice dynamics in Patagonia and on the Antarctic Peninsula. *Palaeogeography, Palaeoclimatology, Palaeoecology*, 162, 357–387. www.elsevier.nl/locate/palaeo

Fang, F.T., Zhu, Z.Y., Wenger, F., Ge, J.Z., Du, J.Z., Deng, B. et al. (2024) Short-term sedimentary evidence for increasing diatoms in Arctic fjords in a warming world. *Science of the Total Environment*, 951, 175757. Available from: https://doi.org/10.1016/j.scitotenv.2024.175757

Flemming, N.C. (1982) Multiple regression analysis of earth movements and eustatic sea-level change in the United Kingdom in the past 9000 years. *Proceedings of the Geologists' Association*, 93(1), 113–125. Available from: https://doi.org/10.1016/S0016-7878(82)80035-7

Gannoun, A. & Burton, K.W. (2014) High precision osmium elemental and isotope measurements of North Atlantic seawater. *Journal of Analytical Atomic Spectrometry*, 29(12), 2330–2342. Available from: https://doi.org/10.1039/c4ja00265b

Gregory, B.R.B., Peros, M., Reinhardt, E.G. & Donnelly, J.P. (2015) Middle-late Holocene Caribbean aridity inferred from foraminifera and elemental data in sediment cores from two Cuban lagoons. *Palaeogeography, Palaeoclimatology, Palaeoecology*, 426, 229–241. Available from: https://doi.org/10.1016/j.palaeo.2015.02.029

Hamilton, C.A., Lloyd, J.M., Barlow, N.L.M., Innes, J.B., Flecker, R. & Thomas, C.P. (2015) Late Glacial to Holocene relative sea-level change in Assynt, northwest Scotland, UK. *Quaternary Research (United States)*, 84(2), 214–222. Available from: https://doi.org/10.1016/j.yqres.2015.07.001

Hou, A., Bahr, A., Raddatz, J., Voigt, S., Greule, M. & Albuquerque, A.L. et al. (2020) Insolation and greenhouse gas forcing of the South American monsoon system across three glacial-interglacial cycles. *Geophysical Research Letters*, 47(14), e2020GL087948. Available from: https://doi.org/10.1029/2020GL087948

Huffman, E., Simms, A.R., Bradwell, T., Best, L., Lloyd, J.M., Bradley, S.L. et al. (2025) New RSL constraints for the Minch from OSL-dated Lateglacial shorelines. *Quaternary Science Reviews*, 367, 109543. Available from: https://doi.org/10.1016/j.quascirev.2025.109543

Isarin, R.F.B. & Renssen, H. (1999) Reconstructing and modelling Late Weichselian climates: the Younger Dryas in Europe as a case study. *Earth-Science Reviews*, 48(1–2), 1–38. Available from: https://doi.org/10.1016/S0012-8252(99)00047-1

Jonk, R., Kelly, J. & Parnell, J. (2004) The origin and tectonic significance of Lewisian- and Torridonian-hosted clastic dykes near Gairloch, NW Scotland. *Scottish Journal of Geology*, 40(2), 123–130. Available from: https://doi.org/10.1144/sjg40020123

Kim, S., Lee, M.K., Shin, J.Y., Yoo, K.C., Lee, J.I., Kang, M.I. et al. (2022) Variation in magnetic susceptibility in the Bellingshausen Sea continental rise since the last glacial period and implications for terrigenous material input mechanisms. *Palaeogeography, Palaeoclimatology, Palaeoecology*, 594, 110948. Available from: https://doi.org/10.1016/j.palaeo.2022.110948

Krabbendam, M. & Bradwell, T. (2014) Quaternary evolution of glaciated gneiss terrains: Pre-glacial weathering vs. glacial erosion. *Quaternary Science Reviews*, 95, 20–42. Available from: https://doi.org/10.1016/j.quascirev.2014.03.013

Kuchar, J., Milne, G., Hubbard, A., Patton, H., Bradley, S., Shennan, I. et al. (2012) Evaluation of a numerical model of the British-Irish ice sheet using relative sea-level data: Implications for the interpretation of trimline observations. *Journal of Quaternary Science*, 27(6), 597–605. Available from: https://doi.org/10.1002/jqs.2552

Kuroda, J., Jiménez-Espejo, F.J., Nozaki, T., Gennari, R., Lugli, S., Manzi, V. et al. (2016) Miocene to Pleistocene osmium isotopic records of the Mediterranean sediments. *Paleoceanography*, 31(1), 148–166. Available from: https://doi.org/10.1002/2015PA002853

Lamb, A.L., Wilson, G.P. & Leng, M.J. (2006) A review of coastal palaeoclimate and relative sea-level reconstructions using δ13C and C/N ratios in organic material. *Earth-Science Reviews*, 75(1–4), 29–57. Available from: https://doi.org/10.1016/j.earscirev.2005.10.003

Levasseur, S., Birck, J.-L. & Allègre, C.J. (1998) Direct measurement of femtomoles of Osmium and the $^{187}Os/^{186}Os$ ratio in seawater. *Science*, 282(5387), 272–274. https://www.science.org

Levasseur, S., Birck, J.-L. & Allègre, C.J. (1999) The osmium riverine flux and the oceanic mass balance of osmium. *Earth and Planetary Science Letters*, 174(1–2), 7–23. Available from: https://doi.org/10.1016/S0012-821X(99)00259-9

Lloyd, J. (2000) Combined foraminiferal and thecamoebian environmental reconstruction from an isolation basin in NW Scotland: Implications for sea-level studies. *Journal of Foraminiferal Research*, 30(4), 294–305. Available from: https://doi.org/10.2113/0300294

Lloyd, J.M. & Evans, J.R. (2002) Contemporary and fossil foraminifera from isolation basins in northwest Scotland. *Journal of Quaternary Science*, 17(5–6), 431–443. Available from: https://doi.org/10.1002/jqs.719

Long, A.J., Barlow, N.L.M., Dawson, S., Hill, J., Innes, J.B., Kelham, C. et al. (2016) Lateglacial and Holocene relative sea-level changes and first evidence for the Storegga tsunami in Sutherland, Scotland.

Journal of Quaternary Science, 31(3), 239–255. Available from: https://doi.org/10.1002/jqs.2862

Lu, X., Kendall, B., Stein, H.J. & Hannah, J.L. (2017) Temporal record of osmium concentrations and 187Os/188Os in organic-rich mudrocks: Implications for the osmium geochemical cycle and the use of osmium as a paleoceanographic tracer. *Geochimica et Cosmochimica Acta*, 216, 221–241. Available from: https://doi.org/10.1016/j.gca.2017.06.046

Nace, T.E., Baker, P.A., Dwyer, G.S., Silva, C.G., Rigsby, C.A., Burns, S.J. et al. (2014) The role of North Brazil Current transport in the paleoclimate of the Brazilian Nordeste margin and paleoceanography of the western tropical Atlantic during the late Quaternary. *Palaeogeography, Palaeoclimatology, Palaeoecology*, 415, 3–13. Available from: https://doi.org/10.1016/j.palaeo.2014.05.030

Paquay, F.S. & Ravizza, G. (2012) Heterogeneous seawater 187Os/188Os during the Late Pleistocene glaciations. *Earth and Planetary Science Letters*, 349–350, 126–138. Available from: https://doi.org/10.1016/j.epsl.2012.06.051

Peucker-Ehrenbrink, B. (2002) Comment on 'residence time of osmium in the oceans' by Rachel Oxburgh. *Geochemistry, Geophysics, Geosystems*, 3(10), 1–4. Available from: https://doi.org/10.1029/2001GC000297

Peucker-Ehrenbrink, B. & Jahn, B. (2001) Rhenium-osmium isotope systematics and platinum group element concentrations: Loess and the upper continental crust. *Geochemistry, Geophysics, Geosystems*, 2(10), 1061-22. Available from: https://doi.org/10.1029/2001GC000172

Peucker-Ehrenbrink, B. & Ravizza, G. (2000) The marine osmium isotope record. *Terra Nova*, 12(5), 205–219. Available from: https://doi.org/10.1046/j.1365-3121.2000.00295.x

Podrecca, L.G., Masterson, A.L., Hurtgen, M.T., Taylor, J., Lloyd, J.M., Selby, D. et al. (2025) Microbial sulfate reduction regulated by relative sea level change in a Pleistocene–Holocene sedimentary record: Insights from Loch Duart, Scotland, UK. *Chemical Geology*, 677, 122633. Available from: https://doi.org/10.1016/j.chemgeo.2025.122633

Ravizza, G. & Turekian, K.K. (1989) Application of the 187Re-187Os system to black shale geochronometry. *Geochimica et Cosmochimica Acta*, 53, 3257–3262.

Rooney, A.D., Selby, D., Lloyd, J.M., Roberts, D.H., Lückge, A., Sageman, B.B. et al. (2016) Tracking millennial-scale Holocene glacial advance and retreat using osmium isotopes: Insights from the Greenland ice sheet. *Quaternary Science Reviews*, 138, 49–61. Available from: https://doi.org/10.1016/j.quascirev.2016.02.021

Rothwell, R.G. & Croudace, I.W. (2015) Twenty years of XRF core scanning marine sediments: What do geochemical proxies tell us? In: Croudace, I. & Rothwell, R. (Eds.) *Micro-XRF studies of sediment cores*. Dordrecht: Springer, pp. 25–102. Available from: https://doi.org/10.1007/978-94-017-9849-5_2

Ruddiman, W.F. & McIntyre, A. (1981) The North Atlantic Ocean during the last deglaciation. *Palaeogeography, Palaeoclimatology, Palaeoecology*, 35, 145–214. Available from: https://doi.org/10.1016/0031-0182(81)90097-3

Sano, J.L., Ratcliffe, K.T. & Spain, D.R. (2013) Chemostratigraphy of the haynesville shale. In: Hammes, U. & Gale, J.F.W. (Eds.) *AAPG Memoir: Geology of the Haynesville Gas Shale in East Texas and West Louisiana*. Tulsa, OK: American Association of Petroleum Geologists, pp. 137–154. Available from: https://doi.org/10.1306/13441847M1053602

Schimmelmann, A., Albertino, A., Sauer, P.E., Qi, H., Molinie, R. & Mesnard, F. (2009) Nicotine, acetanilide and urea multi-level2H-,13C- and15N-abundance reference materials for continuous-flow isotope ratio mass spectrometry. *Rapid Communications in Mass Spectrometry*, 23(22), 3513–3521. Available from: https://doi.org/10.1002/rcm.4277

Scourse, J., Saher, M., Van Landeghem, K.J.J., Lockhart, E., Purcell, C., Callard, L. et al. (2019) Advance and retreat of the marine-terminating Irish Sea Ice Stream into the Celtic Sea during the Last Glacial: Timing and maximum extent. *Marine Geology*, 412, 53–68. Available from: https://doi.org/10.1016/j.margeo.2019.03.003

Selby, D. & Creaser, R.A. (2003) Re-Os geochronology of organic rich sediments: An evaluation of organic matter analysis methods. *Chemical Geology*, 200(3–4), 225–240. Available from: https://doi.org/10.1016/S0009-2541(03)00199-2

Sharma, M., Papanastassiou, D.A. & Wasserburg, G.J. (1997) The concentration and isotopic composition of osmium in the oceans. *Geochimica et Cosmochimica Acta*, 61(16), 3287–3299.

Shemesh, A., Burckle, L.H. & Froelich, P.N. (1989) Dissolution and Preservation of Antarctic Diatoms and the Effect on Sediment Thanatocoenoses. *Quaternary Research*, 31(2), 288–308. Available from: https://doi.org/10.1016/0033-5894(89)90010-0

Shennan, I., Bradley, S.L. & Edwards, R. (2018) Relative sea-level changes and crustal movements in Britain and Ireland since the Last Glacial Maximum. *Quaternary Science Reviews*, 188, 143–159. Available from: https://doi.org/10.1016/j.quascirev.2018.03.031

Shennan, I., Bradley, S., Milne, G., Brooks, A., Bassett, S. & Hamilton, S. (2006a) Relative sea-level changes, glacial isostatic modelling and ice-sheet reconstructions from the British Isles since the Last Glacial Maximum. *Journal of Quaternary Science*, 21(6), 585–599. Available from: https://doi.org/10.1002/jqs.1049

Shennan, I., Hamilton, S., Hillier, C., Hunter, A., Woodall, R., Bradley, S. et al. (2006b) Relative sea-level observations in western Scotland since the Last Glacial Maximum for testing models of glacial isostatic land movements and ice-sheet reconstructions. *Journal of Quaternary Science*, 21(6), 601–613. Available from: https://doi.org/10.1002/jqs.1048

Shennan, I., Hamilton, S., Hillier, C. & Woodroffe, S. (2005) A 16 000-year record of near-field relative sea-level changes, northwest Scotland, United Kingdom. *Quaternary International*, 133–134(1 SUPPL.), 95–106. Available from: https://doi.org/10.1016/j.quaint.2004.10.015

Shennan, I., Lambeck, K., Horton, B., Innes, J., Lloyd, J., Mcarthur, J. et al. (2000) Late Devensian and Holocene records of relative sea-level changes in northwest Scotland and their implications for glacio-hydro-isostatic modelling. *Quaternary Science Reviews*, 19(11), 1103–1135.

Simms, A.R., Best, L., Shennan, I., Bradley, S.L., Small, D., Bustamante, E. et al. (2022) Investigating the roles of relative sea-level change and glacio-isostatic adjustment on the retreat of a marine based ice stream in NW Scotland. *Quaternary Science Reviews*, 277, 107366. Available from: https://doi.org/10.1016/j.quascirev.2021.107366

Smith, D.E., Barlow, N.L.M., Bradley, S.L., Firth, C.R., Hall, A.M., Jordan, J.T. et al. (2019) Quaternary sea level change in Scotland. *Earth and Environmental Science Transactions of the Royal Society of Edinburgh*, 110(1–2), 219–256. Available from: https://doi.org/10.1017/S1755691017000469

Taylor, J., Selby, D., Lloyd, J.M., Podrecca, L., Masterson, A.L., Sageman, B.B. et al. (2024) Palaeoenvironmental reconstruction of Loch Duart (NW Scotland, UK) since the Last Glacial Maximum: implications from a multiproxy approach. *Journal of Quaternary Science*, 39(1), 6–23. Available from: https://doi.org/10.1002/jqs.3566

Taylor, J., Selby, D., Lloyd, J.M., Smeaton, C., Bendle, J. & Allison, M. et al. (2025) Palaeoenvironmental reconstruction of a fjord catchment NW Scotland, UK since the Last Glacial Maximum: A multi-geochemical approach. *Quaternary Science Reviews*, 356, 109311. Available from: https://doi.org/10.1016/j.quascirev.2025.109311

Tisserand, A., Malaizé, B., Jullien, E., Zaragosi, S., Charlier, K. & Grousset, F. (2009) African monsoon enhancement during the penultimate glacial period (MIS 6.5 ~ 170 ka) and its atmospheric impact. *Paleoceanography*, 24(2), PA2220. Available from: https://doi.org/10.1029/2008PA001630

Van Hoang, L., Clift, P.D., Schwab, A.M., Huuse, M., Nguyen, D.A. & Zhen, S. (2010) Large-scale erosional response of SE Asia to monsoon evolution reconstructed from sedimentary records of the Song Hong-Yinggehai and Qiongdongnan basins, South China Sea. *Geological Society, London, Special Publications*, 342(1), 219–244. Available from: https://doi.org/10.1144/SP342.13